Earth and Planetary Science Letters 450 (2016) 317–325

Contents lists available at ScienceDirect

Earth and Planetary Science Letters

www.elsevier.com/locate/epsl

The impact of degassing on the oxidation state of basaltic magmas: A case study of Kīlauea volcano

Yves Moussallam [a,*], Marie Edmonds [b], Bruno Scaillet [c], Nial Peters [d], Emanuela Gennaro [c], Issy Sides [b], Clive Oppenheimer [d]

[a] Geosciences Research Division, Scripps Institution of Oceanography, UCSD, La Jolla, CA 92093-0244, USA
[b] Department of Earth Sciences, University of Cambridge, Downing Street, Cambridge, CB2 3EQ, UK
[c] ISTO, UMR 7327, Université d'Orléans-CNRS-BRGM, 1A rue de la Férollerie, 45071 Orléans cedex 2, France
[d] Department of Geography, University of Cambridge, Downing Place, Cambridge, CB2 3EN, UK

ARTICLE INFO

Article history:
Received 29 March 2016
Received in revised form 17 May 2016
Accepted 17 June 2016
Available online xxxx
Editor: T.A. Mather

Keywords:
oxygen fugacity
sulfur
degassing
XANES
melt inclusions
CO_2

ABSTRACT

Volcanic emissions link the oxidation state of the Earth's mantle to the composition of the atmosphere. Whether the oxidation state of an ascending magma follows a redox buffer – hence preserving mantle conditions – or deviates as a consequence of degassing remains under debate. Thus, further progress is required before erupted basalts can be used to infer the redox state of the upper mantle or the composition of their co-emitted gases to the atmosphere. Here we present the results of X-ray absorption near-edge structure (XANES) spectroscopy at the iron K-edge carried out for a series of melt inclusions and matrix glasses from ejecta associated with three eruptions of Kīlauea volcano (Hawai'i). We show that the oxidation state of these melts is strongly correlated with their volatile content, particularly in respect of water and sulfur contents. We argue that sulfur degassing has played a major role in the observed reduction of iron in the melt, while the degassing of H_2O and CO_2 appears to have had a negligible effect on the melt oxidation state under the conditions investigated. Using gas–melt equilibrium degassing models, we relate the oxidation state of the melt to the composition of the gases emitted at Kīlauea. Our measurements and modelling yield a lower constraint on the oxygen fugacity of the mantle source beneath Kīlauea volcano, which we infer to be near the nickel nickel-oxide (NNO) buffer. Our findings should be widely applicable to other basaltic systems and we predict that the oxidation state of the mantle underneath most hotspot volcanoes is more oxidised than that of the associated lavas. We also suggest that whether the oxidation states of a basalt (in particular MORB) reflects that of its source, is primarily determined by the extent of sulfur degassing.

1. Introduction

The redox state of basalts, and especially of mid ocean ridge basalts (MORBs) has been proposed to be a direct reflection of the oxidation state of their source region (e.g. Carmichael and Ghiorso, 1986; Carmichael, 1991; Bezos and Humler, 2005; Lee et al., 2005; Cottrell and Kelley, 2011). Very slight variations in the oxidation state of MORBs and, by inference, the oxidation state of the upper mantle, have been used to support far-reaching implications of element cycling at the planetary scale (Cottrell and Kelley, 2013; Shorttle et al., 2015). There are several reasons, however, why the oxidation state of erupted MORBs might not reflect mantle conditions. Nearly all MORBs are vapour-saturated and are therefore significantly degassed by the time they erupt (e.g. Moore, 1979; Dixon et al., 1988; Bottinga and Javoy, 1990).

The degassing of volatile species has long been suggested to affect melt oxidation state. The degassing of H_2O and H_2 is predicted to result in a net oxidation of the melt (Sato and Wright, 1966; Sato, 1978; Mathez, 1984; Holloway, 2004); evidence of this process has been observed in rhyolitic melt decompression experiments (Humphreys et al., 2015) but its occurrence in nature remains questionable (Waters and Lange, 2016). The degassing of carbon monoxide may oxidise the melt (Mathez, 1984), while the degassing of sulfur species can oxidise or reduce melts depending on sulfur speciation in the melt (S^{2-} or S^{6+}) and fluid phase (H_2S, or SO_2) (Anderson and Wright, 1972; Carmichael, 1991; Gerlach, 1993; Gaillard and Scaillet, 2009; Métrich et al., 2009; Gaillard et al., 2011, 2015; Kelley and Cottrell, 2012; Moussallam et al., 2014).

* Corresponding author.
E-mail address: ymoussallam@ucsd.edu (Y. Moussallam).

http://dx.doi.org/10.1016/j.epsl.2016.06.031

Similar to MORB, the oxidation state of the mantle feeding ocean island basaltic (OIB) volcanoes has been inferred from the oxidation state of erupted lavas and gases. In Hawai'i these approaches have led to disagreement, with the initial oxidation state of parental Hawaiian magmas argued to be close to the magnetite–wüstite (MW) buffer (Roeder et al., 2003; Rhodes and Vollinger, 2005); close to the nickel nickel-oxide (NNO) buffer (Helz and Thornber, 1987); or close to the quartz–fayalite–magnetite (QFM) buffer (Fudali, 1965; Peck and Wright, 1966; Sato and Wright, 1966; Wright and Weiblen, 1968; Anderson and Wright, 1972; Gerlach, 1980, 1993; Carmichael and Ghiorso, 1986). To date the oxidation state of the Hawaiian mantle plume remains undetermined.

Here, we examine a series of olivine-hosted melt inclusions (MI) and matrix glasses from tephra erupted during three eruptions of Kīlauea volcano. These MI and glasses provide samples of the melt tapped at different degassing stages and have already been extensively characterised in terms of major, trace and volatile element compositions (Edmonds et al., 2013; Sides et al., 2014). We present X-ray absorption near-edge structure (XANES) spectroscopy measurements at the iron K-edge on a subset of these glasses to investigate the link between melt oxidation state and degassing, thereby enabling us to extrapolate back to the mantle oxidation state of pristine, undegassed Kīlauea basalt.

2. Methodology

We began our investigation with a sample set of 387 MI and 175 glasses from 25 historical eruptions at Kīlauea, which had previously been analysed for major, trace and volatile elements by EMP, SIMS and LA-ICPMS by Sides et al. (2014) and Edmonds et al. (2013). From this sample set we selected 20 MI and 24 matrix glasses for XANES spectroscopy measurements at the iron K-edge. The MI were selected based on their calculated amount of post-entrapment crystallisation (PEC) (i.e. from the 387 MI of the sample set we selected the ones with the lowest amount of PEC). This narrowed the sample set to three eruptions, which took place in 2010, 2008 and 1885.

The matrix glasses were then taken from corresponding eruptions. The 2010 and 2008 samples are from transient explosive (gas-rich, melt-poor) eruptions and consist of pumiceous bombs/lapilli and lithics, while the 1885 samples relate to an effusive eruption and taken from the upper 1–1.5 cm of the glass-rich vesicular rope texture on pāhoehoe lava flow surfaces. The melt composition of these three eruptions is representative of typical Kīlauea basalt (Fig. S1). The selected samples were re-polished to remove the spot left by previous SIMS analysis and polished on the reverse side in order to obtain doubly-exposed wafers with at least a 10×10 μm^2 obstruction-free area through the inclusion. Fig. 1 shows the typical morphology of an olivine-hosted MI and its surrounding glass. The analysed inclusions vary in size from 20 to 60 μm across and consist of brown-coloured transparent glass of ovoid shape located throughout the crystal.

2.1. XANES data acquisition

All samples were analysed on Beamline I18 at the diamond light source (DLS) using Fe K-edge XANES (X-ray absorption near-edge structure spectroscopy). The X-rays were focused with Kirkpatrick–Baez mirrors down to 2 μm (horizontal) ×2.5 μm (vertical) beam size. The beamline utilises a liquid nitrogen-cooled double-crystal monochromator with silicon crystals and Si(333) reflection was used to increase the energy resolution. Measurements were performed in fluorescence mode and the energy-dispersive detector used was a 6-element SGX Sensortech silicon drift detector positioned at 90° to the incident X-ray beam. The sample was positioned so that the normal to the sample surface was at 10° to the incident X-ray beam to improve the horizontal resolution and reduce potential self-absorption effects. The incident X-ray beam was filtered with Al foils (varying in thickness from 0.025 to 0.1 mm) to keep the detector count rate within the linear response region and to remove the effect of beam damage on the sample. The energy step sizes and dwell times used are given in Table S1.

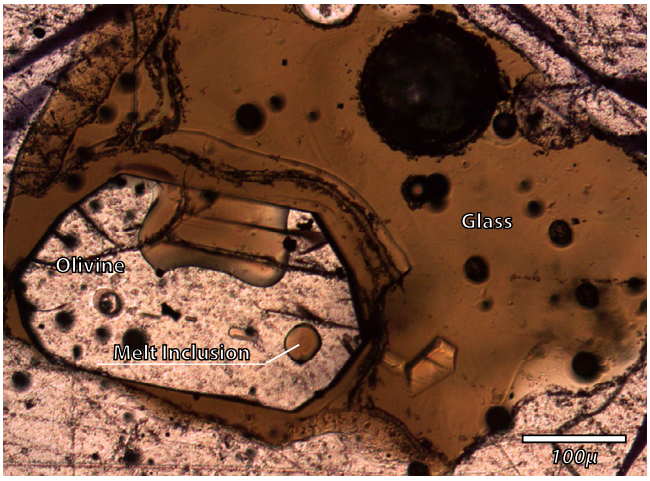

Fig. 1. Transmitted light photomicrograph of an olivine hosted melt inclusion from the 2010 eruption (sample S3-56). Rapid quenching of the MI and matrix glass is evident from the absence of microlites and is representative of all three eruptions investigated.

2.2. Beam damage

Focused beams of X-rays have been shown to either reduce (Wilke et al., 2008; Métrich et al., 2009) or oxidise (Moussallam et al., 2014) sulfur during XANES analyses on a timescale of minutes. The effect of beam damage at the Fe K-edge has been investigated in several studies (Cottrell et al., 2009; Moussallam et al., 2014; Shorttle et al., 2015). Cottrell et al. (2009) and Moussallam et al. (2014) found no effect of prolonged beam-time on the Fe speciation under their set of analytical conditions. Shorttle et al. (2015) found that under certain analytical conditions (without attenuation of the beam) a small amount of photo-oxidation could be generated over the first 12 min of sample exposure to the beam. In order to determine if beam damage was occurring under our analytical conditions we acquired five successive spectra on a natural Kīlauea glass sample. Spectra were obtained using a "fast-scanning" mode such that each spectrum took about 4.5 min to acquire. Although "fast-scanning" results in lower resolution spectra it allows investigation of time-dependent beam damage. Apart from shorter dwell time, these spectra were acquired under the same analytical conditions as the rest of the sample set and using an Al plate of 0.025 mm. Fig. S2 shows that all five spectra are nearly identical and hence that no significant beam damage is to be expected in our analyses.

2.3. Spectral processing and $Fe^{3+}/\sum Fe$ calibration

The pre-edge region (7110–7118 eV) on a XANES spectrum at the Fe K-edge corresponds to the $1s \rightarrow 3d$ electronic transition. The pre-edge region was fitted using a combination of a linear function and a damped harmonic oscillator function (DHO) to fit the baseline (Cottrell et al., 2009; Moussallam et al., 2014) (Fig. S3). The centroid (area-weighted average) of the background-subtracted pre-edge region was then calculated and parametrised against the Fe valence state. We used the NMNH 117393 basalt reference glasses (Cottrell et al., 2009) loaned by the Smithsonian Institution

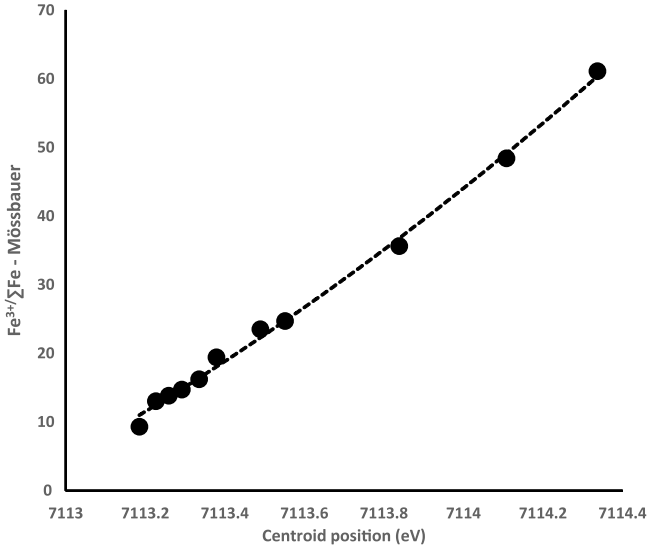

Fig. 2. Calibration curve of the centroid position determined by XANES compared with the $Fe^{3+}/\sum Fe$ ratios in standard glasses determined by Mößbauer spectroscopy (from Cottrell et al., 2009).

National Museum of Natural History to calibrate the $Fe^{3+}/\sum Fe$ ratio in the unknown samples. The reference glasses were analysed at the beginning and end of the session and an average spectrum for each glass was used to derive the calibration curve.

We found no drift occurring between the two analyses and in fact no drift since our analysis of the same standards the previous year (session reported in Shorttle et al., 2015). The standard deviation between repeated analyses was used to determine the error on the centroid position ($1\sigma = 0.011$ eV) which translates to a standard deviation of 0.4% on the measured $Fe^{3+}/\sum Fe$ ratio. We note that this error is solely associated with the XANES analyses. The absolute error on the $Fe^{3+}/\sum Fe$ ratio will depend on the error associated with the initial Mößbauer analyses of the reference glasses. Recently, Berry et al. (2015) have drawn attention to the $Fe^{3+}/\sum Fe$ ratio determined by Mößbauer in Cottrell et al. (2009) and proposed alternative values. At the time of writing it is unclear which of these absolute determinations is correct and we choose here to use the Cottrell et al. (2009) Mößbauer values. If future studies demonstrate that these values are incorrect, our results can readily be recalculated. The calibration curve is presented in Fig. 2. All XANES spectra of MI were examined for contamination from the olivine host. Spectra showing any structure in the edge and post edge region were rejected.

2.4. Gas–melt equilibrium modelling

In order to relate the oxidation state of the melt to that of the gas phase and to explore the theoretical effect of closed-system degassing on the oxidation state of both phases, we modelled several equilibrium scenarios. The model used in this study is described in Gaillard and Scaillet (2009) and Gaillard et al. (2011) and solves, at each pressure step, the following reactions in the C–H–S–O system, at magmatic pressure and temperature:

$$CO_{(gas)} + 1/2O_2 = CO_{2(gas)} \quad (1)$$

$$H_{2(gas)} + 1/2O_2 = H_2O_{(gas)} \quad (2)$$

$$CH_{4(gas)} + 2O_2 = CO_{2(gas)} + 2H_2O_{(gas)} \quad (3)$$

$$1/2S_{2(gas)} + O_2 = SO_{2(gas)} \quad (4)$$

$$1/2S_{2(gas)} + H_2O_{(gas)} = H_2S_{(gas)} + 1/2O_2 \quad (5)$$

The gas–melt equilibria, using thermodynamic data for water and carbon dioxide (Iacono-Marziano et al., 2012), sulfur (O'Neill and Mavrogenes, 2002) and hydrogen (Gaillard et al., 2003), are dictated by the following reactions:

$$H_2O_{(gas)} + O^{2-}_{(melt)} = 2OH^-_{(melt)} \quad (6)$$

$$CO_{2(gas)} + O^{2-}_{(melt)} = CO_3{}^{2-}_{(melt)} \quad (7)$$

$$S_{2(gas)} + 2O^{2-}_{(melt)} = O_2 + 2S^{2-}_{(melt)} \quad (8)$$

$$H_{2(gas)} = H_{2(melt)} \quad (9)$$

The iron redox ratio in the melt is computed using Kress and Carmichael (1991):

$$\ln\left(\frac{XFe_2O_3}{XFeO}\right) = a\ln(fO_2) + \frac{b}{T} + c + \sum d_i X_i \quad (10)$$

where $a = 0.196$, $b = 11492$, $c = -6.675$, $d_{Al_2O_3} = -2.243$, $d_{FeO} = -1.828$, $d_{Na_2O} = 5.854$, $d_{K_2O} = 6.215$ and $d_{CaO} = 3.201$.

3. Results

XANES results are reported in Table 1; example spectra from natural glasses and from standard glasses are presented in Fig. 3. The calculated $Fe^{3+}/\sum Fe$ ratios are shown for all three eruptions in Fig. 4. Results from the 2008 and 2010 eruptions indicate a strong correlation between the amount of dissolved sulfur and water and the glass oxidation state (r^2 values of 0.75 and 0.8 respectively) and a very weak correlation between the amount of dissolved CO_2 and the glass oxidation state (r^2 values of 0.3). Taken separately, the correlation between sulfur content and the glass oxidation state for the 2010 eruption sample is very weak (r^2 values of 0.2) but this reflects the limited dataset for this event. MI and glasses from the 1885 eruption show little to no correlation between the amount of sulfur dissolved and the glass oxidation state, no correlation between the amount of water dissolved and the glass oxidation state and a clear correlation between the amount of CO_2 dissolved and the glass oxidation state. In all cases, MI and glasses containing higher concentrations of volatiles are more oxidised than MI and glasses containing lower volatile abundances. Degassing of volatile elements at Kīlauea therefore appears to be consistently associated with a reduction of the melt.

4. Discussion and modelling

4.1. Crystallisation of Fe-bearing minerals

Degassing is not the only mechanism that influences the oxidation state of a melt. For instance, the crystallisation of Fe-bearing species such as olivine, magnetite and pyrrhotite has a strong influence (e.g. Carmichael and Ghiorso, 1990). However, we can exclude crystallisation of Fe-bearing minerals, and indeed differentiation in general, as the driving force behind the observed reducing trend since there is no correlation between the melt iron content or Mg number and its oxidation state (Fig. S4). Fig. S4 also shows the lack of correlation between the estimated amounts of PEC and the MI oxidation state, demonstrating that the measured redox signal is not influenced by post-entrapment crystallisation.

4.2. Volatile degassing modelling

The degassing of both water and carbon species is expected to result in a net oxidation of the melt if H_2 and CO species are preferentially degassed (Sato and Wright, 1966; Sato, 1978; Mathez, 1984; Candela, 1986; Holloway, 2004). Since the relationship we observe between these two species and the glass oxidation

Table 1
Centroid position, $Fe^{3+}/\sum Fe$, ΔQFM (calculated using the $Fe^{3+}/\sum Fe$ ratio and the equation of Kress and Carmichael, 1991) and calculated pressure (using Iacono-Marziano et al., 2012) for all melt inclusions and glasses analysed together with volatile content and major element composition (from Sides et al., 2014).

Eruption date	Sample name	Sample type	Centroid energy	1σ	$Fe^{3+}/\sum Fe$	1σ	Delta QFM	CO_2 (ppm)	1σ	H_2O (wt%)	1σ	Sulfur (ppm)	1σ	Pressure (bar)	1σ	SiO_2	TiO_2	Al_2O_3	Cr_2O_3	FeO	MnO	MgO	CaO	Na_2O	NiO	K_2O	P_2O_5	F	Cl	SO_2	Total	PEC Ol%	Fo host	Mg#
Kilauea 1885	1885A-15m1	MI	7113.282	0.011	0.14	0.004	−0.25		n.d	0.10	0.00	176	8			49.7	2.8	14.2	0.02	11.3	0.19	5.7	12.1	2.42	0.00	0.46	0.29	0.059	0.011	0.04	99.3	3.1	78.8	50
	1885A-og21	Glass	7113.257	0.011	0.14	0.004	−0.35		n.d	0.14	0.01	157	7			51.0	3.1	13.2	0.03	12.2	0.18	6.2	10.9	2.60	0.01	0.62	0.31	0.062	0.013	0.03	100.5			50
	1885B-12m2	MI	7113.291	0.011	0.15	0.004	−0.30	180	12	0.10	0.00	944	41	535	8	50.1	2.8	14.3	0.04	9.7	0.15	6.7	12.5	2.54	0.02	0.56	0.34	0.057	0.017	0.19	99.9	5.6	80.9	58
	1885B-14m1	MI	7113.264	0.011	0.14	0.004	−0.34	95	7	0.13	0.01	226	10	297	4	50.1	2.8	13.5	0.03	11.7	0.20	6.2	11.5	2.43	0.01	0.56	0.29	0.057	0.012	0.05	99.5	0.4	77.6	51
	1885B-14m2	MI	7113.282	0.011	0.14	0.004	−0.22	59	4	0.12	0.01	209	10	190	3	50.5	2.8	13.6	0.04	12.0	0.19	5.5	11.8	2.33	0.00	0.56	0.29	0.055	0.011	0.04	99.7	1.9	77.6	47
	1885B-16m1	MI	7113.278	0.011	0.14	0.004	−0.25		n.d	0.09	0.00	176	8			51.2	3.0	13.4	0.02	11.8	0.21	6.0	11.2	2.69	0.00	0.57	0.31	0.069	0.015	0.04	100.4	1.8	78.3	50
	1885A-26m1	MI	7113.282	0.011	0.14	0.004	−0.27		n.d	0.10	0.00	171	8			50.6	3.4	13.6	0.03	12.0	0.19	4.5	11.9	2.65	0.01	0.63	0.34	0.067	0.013	0.03	100.0	3.9	77.5	43
	1885A-g03	Glass	7113.243	0.011	0.13	0.004	−0.46		n.d	0.13	0.01	165	8			50.5	3.1	13.2	0.02	11.8	0.18	6.3	10.9	2.59	0.02	0.60	0.31	0.058	0.015	0.03	99.7			52
	1885B-og02	Glass	7113.246	0.011	0.13	0.004	−0.43		n.d	0.09	0.00	135	6			50.8	3.0	13.3	0.03	12.2	0.17	6.4	10.9	2.65	0.00	0.59	0.31	0.058	0.015	0.03	100.5			51
	1885B-og12	Glass	7113.245	0.011	0.13	0.004	−0.47		n.d	0.11	0.01	139	6			50.4	3.0	13.3	0.02	11.3	0.18	6.3	11.1	2.60	0.00	0.57	0.30	0.054	0.015	0.03	99.3			52
Kilauea 2010	S3-14m1	MI	7113.368	0.011	0.18	0.004	0.36	99	7	0.18	0.01	468	21	308	4	51.8	2.3	13.5	0.05	11.1	0.16	7.1	10.9	2.33	0.01	0.42	0.22	0.038	0.007	0.09	100.0	4.3	81.7	56
	S3-24m1	MI	7113.285	0.011	0.15	0.004	−0.14	151	10	0.22	0.01	703	31	462	7	52.1	2.3	13.6	0.05	10.8	0.17	7.2	10.7	2.38	0.04	0.45	0.25	0.038	0.007	0.14	100.3	4.6	81.5	57
	S3-56m1	MI	7113.304	0.011	0.15	0.004	0.00	76	5	0.16	0.01	976	44	240	3	51.4	2.4	13.8	0.05	11.8	0.17	7.1	11.0	2.34	0.02	0.43	0.25	0.041	0.011	0.20	101.0	3.5	81.7	54
	S3-57m1	Emb	7113.271	0.011	0.14	0.004	−0.23		n.d	0.15	0.01	509	23			51.7	2.4	13.8	0.05	11.5	0.18	6.9	11.1	2.36	0.01	0.39	0.24	0.048	0.009	0.10	100.9	4.2	81.3	54
	2010-S3-g04	Glass	7113.269	0.011	0.14	0.004	−0.24		n.d	0.09	0.00	231	11			51.8	2.4	13.5	0.04	11.2	0.17	7.3	10.9	2.30	0.00	0.41	0.23	0.042	0.008	0.05	100.4			57
	2010-S3-g56	Glass	7113.255	0.011	0.13	0.004	−0.32		n.d	0.11	0.01	184	9			51.2	2.3	13.7	0.05	11.0	0.17	7.5	10.8	2.31	0.02	0.39	0.22	0.030	0.011	0.04	99.8			57
	2010-S3-g57	Glass	7113.244	0.011	0.13	0.004	−0.39		n.d	0.08	0.00	174	8			51.6	2.4	13.6	0.06	11.6	0.18	7.5	10.9	2.32	0.02	0.41	0.23	0.039	0.009	0.03	100.8			56
Kilauea 2008	18-01m2	MI	7113.358	0.011	0.17	0.004	0.26		n.d	0.28	0.01	693	31			49.9	2.4	13.3	0.06	11.1	0.19	7.5	10.9	2.64	0.03	0.41	0.24	0.044	0.008	0.14	98.9	2.7	82.0	57
	18-07m1	MI	7113.394	0.011	0.19	0.004	0.54		n.d	0.31	0.02	953	43			50.9	2.4	13.5	0.04	11.7	0.19	7.6	10.8	2.37	0.02	0.42	0.23	0.041	0.008	0.19	100.3	2.2	81.8	56
	18-13m2	MI	7113.408	0.011	0.19	0.004	0.60		n.d		n.d	1570	71			50.2	2.5	13.3	0.05	11.0	0.19	7.5	10.9	2.22	0.02	0.37	0.27	0.046	0.008	0.31	98.9	2.9	82.0	57
	18-22m1	MI	7113.331	0.011	0.16	0.004	0.12	145	9	0.26	0.01	397	18	445	6	51.2	2.4	13.6	0.05	10.8	0.20	7.3	11.1	2.34	b.d	0.43	0.23	0.047	0.012	0.08	98.7	4.2	82.1	57
	18-23m1	MI	7113.279	0.011	0.14	0.004	−0.21	233	15	0.18	0.01	600	26	696	10	51.2	2.5	13.6	0.04	11.3	0.19	6.7	11.3	2.49	0.01	0.36	0.22	0.039	0.009	0.12	100.1	5.7	82.3	54
	18-25m1	MI	7113.343	0.011	0.17	0.004	0.19	239	16	0.25	0.01	1304	58	701	11	50.8	2.4	13.5	0.06	11.4	0.18	7.0	11.3	2.42	0.02	0.38	0.22	0.044	0.012	0.26	100.1	5.0	82.5	55
	2008-18-gb1	Glass	7113.248	0.011	0.13	0.004	−0.39		n.d	0.09	0.00	167	8			51.5	2.4	13.5	0.04	11.3	0.17	7.6	10.9	2.40	0.02	0.43	0.22	0.027	0.008	0.03	100.7			57
	2008-18-og07	Glass	7113.248	0.011	0.13	0.004	−0.39		n.d	0.11	0.01	144	7			51.7	2.4	13.4	0.05	11.0	0.17	7.4	10.8	2.37	0.01	0.41	0.23	0.030	0.007	0.03	100.1			57
	2008-18-og19	Glass	7113.282	0.011	0.14	0.004	−0.14		n.d		n.d	219	10			51.7	2.4	13.7	0.08	11.3	0.20	7.5	10.9	2.34	0.02	0.40	0.22	0.030	0.008	0.04	100.9			57
	2008-18-og25	Glass	7113.300	0.011	0.15	0.004	−0.03		n.d		n.d	201	9			51.7	2.5	13.6	0.04	11.1	0.18	7.4	10.9	2.32	0.02	0.39	0.24	0.029	0.009	0.04	100.3			57
	S2-44m1	MI	7113.336	0.011	0.16	0.004	0.19	110	7	0.24	0.01	777	34	344	5	51.5	2.4	13.5	0.05	11.0	0.16	7.3	10.9	2.22	0.01	0.40	0.23	0.043	0.008	0.16	99.9	5.4	82.5	57
	2008-S2-g44	Glass	7113.271	0.011	0.14	0.004	−0.23		n.d	0.11	0.01	234	11			52.1	2.4	13.6	0.04	11.0	0.16	7.6	10.8	2.35	0.01	0.42	0.23	0.034	0.008	0.05	100.7			58
	S2-38m1	MI	7113.375	0.011	0.18	0.004	0.44	71	5	0.29	0.01	1237	55	234	3	51.5	2.3	13.9	0.04	11.4	0.17	7.3	10.6	2.41	0.02	0.41	0.23	0.042	0.009	0.25	100.5	4.6	82.4	56
	2008-S2-g38	Glass	7113.248	0.011	0.13	0.004	−0.38		n.d	0.09	0.00	167	8			51.8	2.4	13.4	0.06	10.9	0.17	7.5	10.7	2.28	0.02	0.42	0.22	0.038	0.007	0.03	100.0			58
	S2-11m1	MI	7113.382	0.011	0.18	0.004	0.45	137	9	0.26	0.01	1170	52	422	6	51.7	2.4	13.6	0.06	11.2	0.18	7.2	11.0	2.25	0.01	0.43	0.23	0.046	0.009	0.23	100.5	5.2	82.3	56
	2008-S2-g11	Glass	7113.274	0.011	0.14	0.004	−0.22		n.d		n.d	234	11			51.7	2.4	13.3	0.05	10.8	0.18	7.5	10.8	2.30	0.02	0.44	0.23	0.036	0.007	0.05	99.8			58
	2008-S2-g03	Glass	7113.254	0.011	0.13	0.004	−0.34		n.d	0.10	0.00	180	8			51.9	2.4	13.5	0.04	11.2	0.17	7.5	10.8	2.33	0.01	0.43	0.23	0.037	0.008	0.04	100.6			57
	S1-24m1	MI	7113.428	0.011	0.20	0.004	0.70	95	6	0.37	0.02	1141	50	316	4	51.8	2.5	13.5	0.04	11.4	0.18	7.2	11.2	2.29	0.02	0.40	0.25	0.040	0.010	0.23	101.0	5.0	82.5	56
	2008-S1-g06	Glass	7113.261	0.011	0.14	0.004	−0.30		n.d		n.d	157	7			51.8	2.4	13.1	0.05	11.5	0.19	7.5	11.1	2.33	0.00	0.41	0.24	0.044	0.010	0.03	100.6			56
	2008-S1-g17	Glass	7113.299	0.011	0.15	0.004	−0.04		n.d		n.d	178	8			51.8	2.4	13.5	0.04	11.0	0.18	7.4	10.8	2.31	0.02	0.41	0.22	0.039	0.009	0.04	100.2			57
	2008-S1-g24	Glass	7113.282	0.011	0.14	0.004	−0.13		n.d		n.d	177	8			51.8	2.4	13.9	0.04	11.3	0.16	7.6	10.9	2.31	0.02	0.41	0.22	0.042	0.007	0.04	101.2			57
	2008-S1-g26	Glass	7113.286	0.011	0.15	0.004	−0.13		n.d	0.09	0.00	209	10			51.5	2.5	13.5	0.05	11.2	0.17	7.4	10.9	2.30	0.01	0.41	0.23	0.039	0.009	0.04	100.3			57
	2008-S1-g47	Glass	7113.275	0.011	0.14	0.004	−0.19		n.d	0.08	0.00	173	8			51.8	2.5	13.3	0.04	11.3	0.16	7.5	10.8	2.31	0.01	0.42	0.23	0.039	0.008	0.03	100.4			57
	2008-S1-g53	Glass	7113.263	0.011	0.14	0.004	−0.27		n.d	0.09	0.00	171	8			52.0	2.5	13.4	0.05	11.1	0.17	7.5	10.8	2.27	0.02	0.42	0.23	0.034	0.009	0.03	100.5			57
	18-29m1	MI	7113.293	0.011	0.15	0.004	−0.06	209	14	0.29	0.01	977	44	628	9	51.2	2.4	13.5	0.05	11.8	0.18	7.0	10.9	2.33	b.d	0.35	0.22	0.047	0.011	0.20	99.2	3.5	81.8	54
	2008-18-g01	Glass	7113.255	0.011	0.13	0.004	−0.33		n.d	0.16	0.01	159	7			51.6	2.4	13.4	0.04	11.3	0.17	7.7	10.8	2.37	0.02	0.41	0.21	0.035	0.008	0.03	100.5			57
	2008-18-g02	Glass	7113.257	0.011	0.14	0.004	−0.33		n.d		n.d	291	13			51.4	2.4	13.5	0.06	11.0	0.18	7.4	10.8	2.39	0.01	0.40	0.24	0.031	0.012	0.06	99.9			56

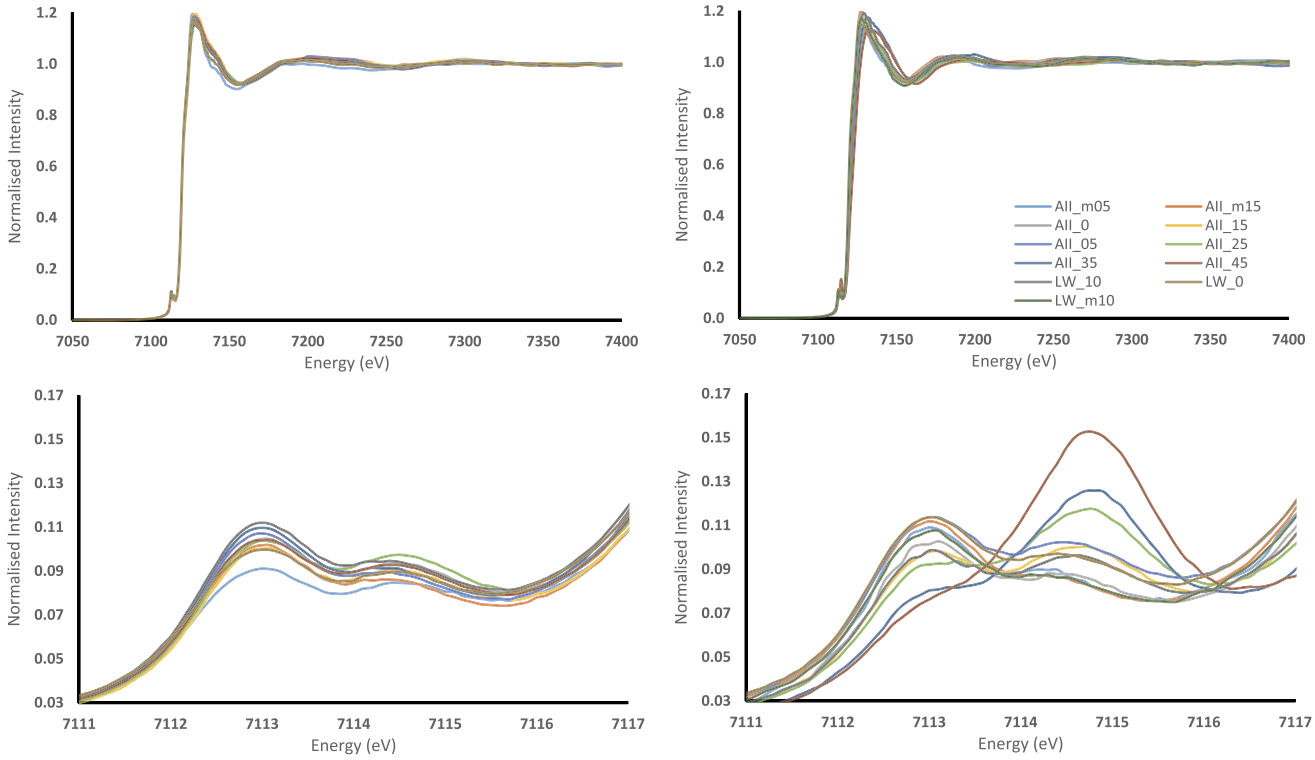

Fig. 3. Edge-step normalised XANES spectra. A: Example spectra for MI and matrix glass from the 2008 eruption. B: Spectra of all standard glasses used in this study. (C) and (D) show spectra over the pre-edge region energy range for sample and standard glasses, respectively.

state is the opposite (reduction with degassing) it would seem that the degassing of neither H_2O nor CO_2 influences melt oxidation state under the explored conditions.

The potential of sulfur degassing to influence the melt oxidation state has been shown theoretically (e.g. Anderson and Wright, 1972; Carmichael and Ghiorso, 1990; Burgisser and Scaillet, 2007; Gaillard and Scaillet, 2009; Métrich et al., 2009; Gaillard et al., 2011) and in nature, at Erebus volcano where a strong reduction of the melt was found to be driven by sulfur degassing (Moussallam et al., 2014). The influence of SO_2 degassing on the oxidation of Kīlauea melts was postulated by Helz (2009) on the basis of apparent disequilibrium between microphenocrysts and carrier liquids (see also Carmichael and Ghiorso, 1986). The correlation observed between sulfur and the $Fe^{3+}/\sum Fe$ ratio in Kīlauea's MI appears to confirm this process.

In order to test this hypothesis, we modified a gas–melt equilibrium model (Gaillard and Scaillet, 2009) to simulate the effect of sulfur degassing on iron speciation. The model starting conditions are reported in Table 2 and degassing is simulated from conditions preserved by the least-degassed MI without adjustment of the model for lower pressure calculations. Fig. 5 shows the results of this gas–melt equilibrium model for all three eruptions. To a first order the model does reproduce the observed reduction of the melt with degassing. In detail, the modelled sulfur *vs.* $Fe^{3+}/\sum Fe$ ratio trends are not quite as steep as those recorded by the data (Fig. 5A). The modelled H_2O *vs.* $Fe^{3+}/\sum Fe$ ratio trends are fairly close to those defined by the samples (Fig. 5B). The modelled CO_2 *vs.* $Fe^{3+}/\sum Fe$ ratio trends do reconcile the observed difference between MI and matrix glasses although a large scatter is apparent in the case of the 2008 MI oxidation state (Fig. 5C).

Since water and sulfur tend to degas in tandem at shallow depths in relatively water-poor basaltic systems, it can be difficult to resolve their respective effects on melt oxidation state. Performing model calculations without sulfur however, results in degassing occurring with no change in the melt oxidation state. It is clear therefore that it is the degassing of sulfur that is responsible for the observed trend of reduction with degassing, as previously shown for the comparatively CO_2-rich Erebus system (Moussallam et al., 2014). The strong correlation between the melt water content and oxidation state is the result of water degassing concurrently with sulfur, as reproduced by the models.

4.3. Comparison with volcanic gases

Despite the constant monitoring performed by the Hawaiian Volcano Observatory, few published studies report the full composition of Kīlauea's gas emissions and none has reported gas composition for the eruptions studied here. Gas compositional data have been reported for the summit lava lake in 1918–1919 (Gerlach, 1980, 1993), the 1983 East Rift zone eruption (Gerlach, 1993), East Rift gases from Pu'u 'Ō'ō in 2004–2005 (Edmonds and Gerlach, 2007) and the summit lava lake during effusive eruption in 2008 (Edmonds et al., 2013). The computed gas composition in equilibrium with a degassing model starting at 2550 m depth is shown in Fig. 6 and compared with gas measurements reported in the literature. To first order, the gas oxidation state (and hence composition) reported in the literature seems to match fairly well with that measured in the melt and modelled. In detail the reported gas compositions span a fairly large range, reflecting the fact that they represent equilibrium with the melt at different temperatures and are generated during both closed- and open-system styles of degassing.

The magma feeding the Kīlauea summit lava lake is probably convecting in the conduit (e.g. Gerlach, 1986; Wallace and Anderson, 1998; Hauri, 2002; Mather et al., 2012; Edmonds et al., 2013). Evidence for this comes in the form of mixing trends in melt inclusion geochemistry (Edmonds et al., 2013), observations of cyclic microgravity (Carbone and Poland, 2012), the high and persistent gas fluxes in the absence of significant volumes of erupted magma, which requires a continuous supply of gas-rich magma to low

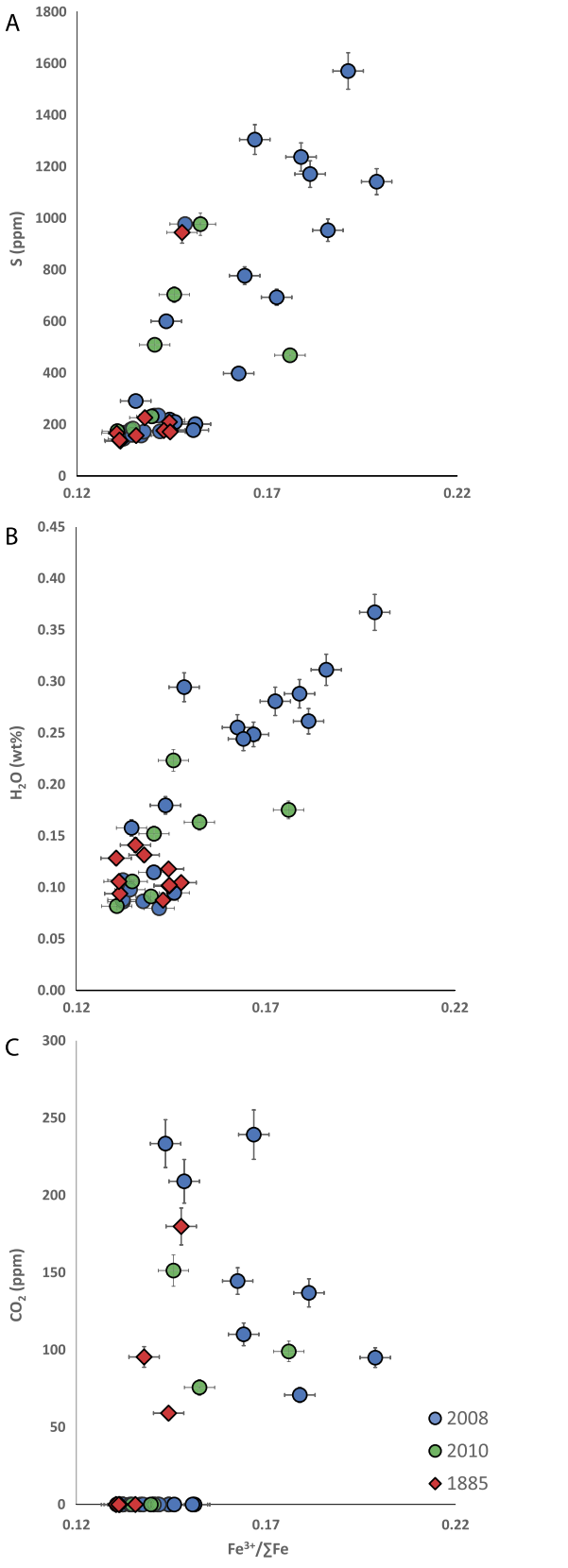

Fig. 4. A: Plot of S concentration (in ppm; determined by EMPA; Sides et al., 2014) compared with the $Fe^{3+}/\sum Fe$ ratio determined by XANES. B: Plot of H_2O concentration (in wt%; determined by SIMS Sides et al., 2014) compared with the $Fe^{3+}/\sum Fe$ ratio determined by XANES. C: Plot of CO_2 concentration (in ppm; determined by SIMS Sides et al., 2014) compared with the $Fe^{3+}/\sum Fe$ ratio determined by XANES.

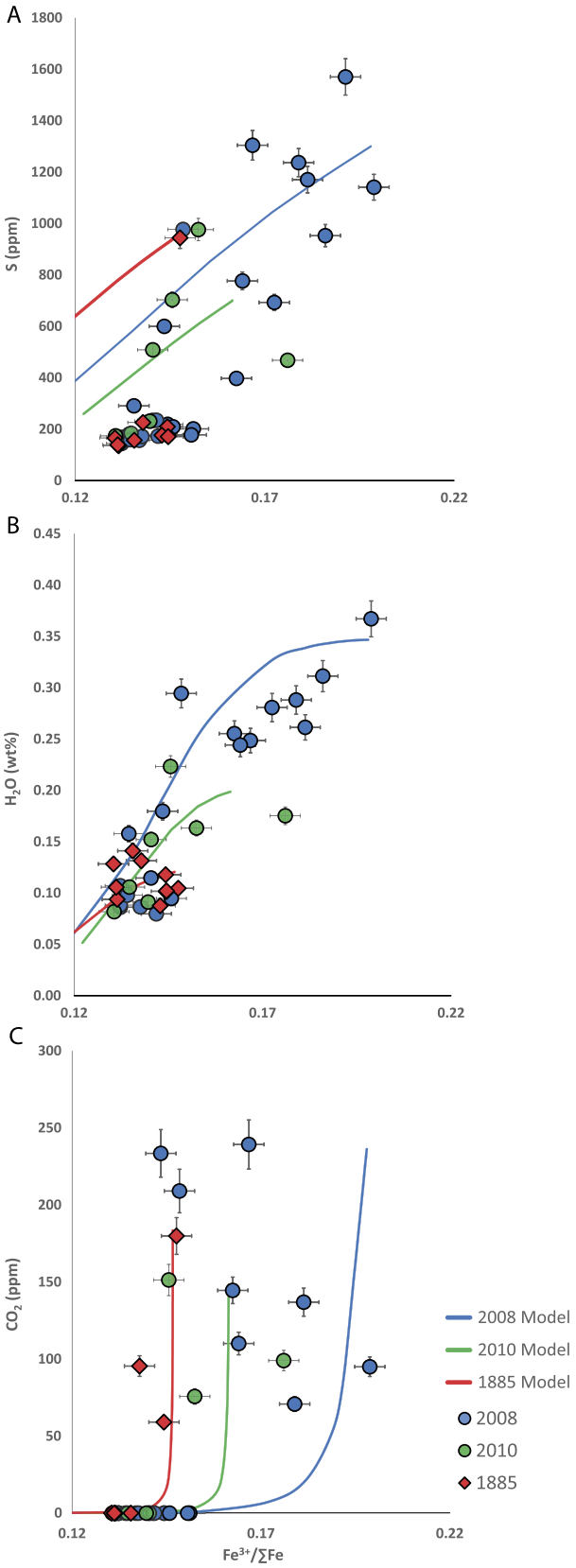

Fig. 5. Plots of S, H_2O and CO_2 concentrations (A, B and C respectively) versus $Fe^{3+}/\sum Fe$ ratio for MI and glasses along with modelled degassing trajectories for each of the three eruptions. The model initial conditions are reported in Table 2.

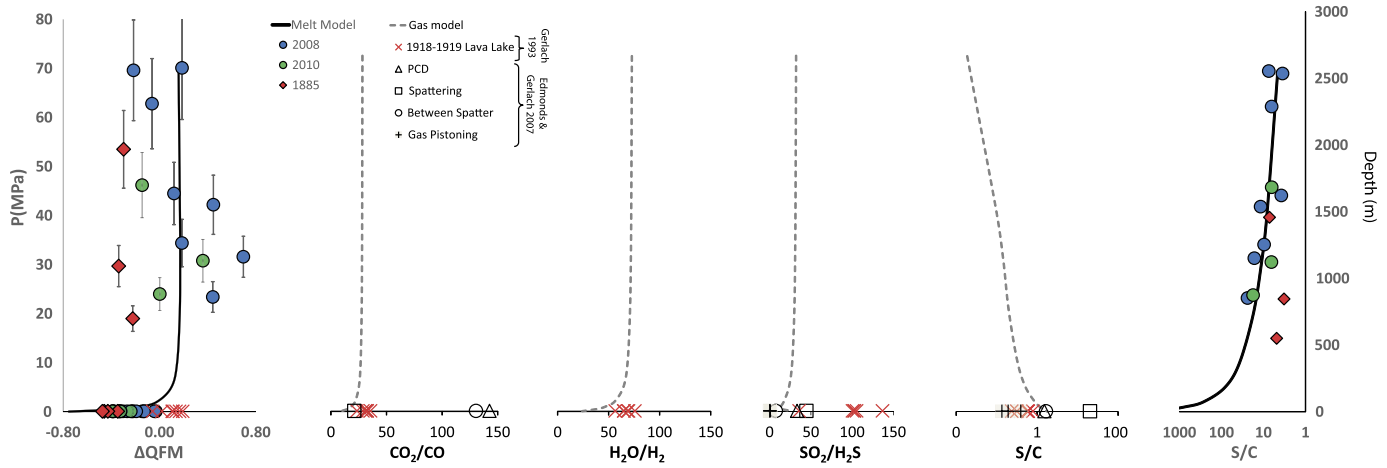

Fig. 6. Calculated fO_2 (as ΔQFM) and volcanic gas redox-couple ratio as a function of pressure. Solid black lines show the result of the gas–melt equilibrium model with respect to the melt and dashed lines show the results for the gas phase. Reported compositions of volcanic gases measured at Kīlauea (Gerlach, 1993; Edmonds and Gerlach, 2007) are shown for comparison.

Table 2
Starting conditions used in for each model run. Sulphur capacity calculated using O'Neill and Mavrogenes (2002). PEC refers to the amount of post entrapment crystallisation as calculated using petrolog3 (Danyushevsky and Plechov, 2011). Fo Host refers to the forsterite content of the MI host olivine.

Model	Pressure (bar)	Temperature (K)	FeO (wt%)	lnCs*	S (ppm)	fH_2O (bar)	fH_2 (bar)
2010	450	1493.15	11.65	−1.58	700	7	0.11
2008	700	1493.15	11.65	−1.58	1300	18	0.15
1885	550	1493.15	11.65	−1.58	950	3	0.063
Degassing	700	1493.15	11.65	−1.58	800	8	0.11

pressures (e.g. Francis et al., 1993; Tazieff, 1994) and observations of lake turnover and downwelling on the lake surface (Patrick et al., 2011). Such a process could result in the recycling of magma batches and crystals (Moussallam et al., 2015) and might explain the scatter observed in the MI oxidation state data with respect to entrapment pressure. Such processes are not captured in our attempt to model degassing as a closed system. In addition, disequilibrium degassing such as that experimentally simulated for Stromboli basalt (Pichavant et al., 2013), might also affect the relative proportions of degassed volatile species. Such a degassing model however, has the potential to faithfully reproduce the natural system in the case of flank eruptions caused by a dyke intrusion without prior shallow degassing of the melt.

It is worth noting that while the oxidation state of the gases broadly agrees with that of the MI entrapped at depth (mean at ∼ΔQFM +0.2 or ∼ΔNNO −0.5), it is not consistent with the oxidation state of the matrix glasses (mean at ∼ΔQFM −0.3 or ∼ΔNNO −1). The mean oxidation state we measured on Kīlauea matrix glasses is very similar to that measured by Carmichael and Ghiorso (1986) (mean at ∼ΔNNO −1.1) and less reduced than that found by Roeder et al. (2003) (mean at ∼ΔNNO −1.7). This discrepancy between the glass and gas oxidation state at Kīlauea had already been pointed out by Gerlach (2004) who argued that the oxidation state of the gas might reflect that of the melt prior to the degassing of sulfur. Roeder et al. (2004) agreed with that interpretation and the data we present here clearly corroborate it. The gas chemistry of Kīlauea's summit lava lake reflects an integrated signal of oxidised gases exsolved at depth and reduced gases exsolved at the near surface.

4.4. Oxidation state of the Hawaiian mantle plume

The oxidation state of the melt inclusions having experienced the least amount of sulfur degassing is close to the nickel nickel-oxide (NNO) buffer. These inclusions are not necessarily the ones recording the highest entrapment pressure because of the convection processes operating at Kīlauea as discussed in section 4.3. However, inclusions preserving high sulfur contents likely preserve redox conditions closest to that of the primary melt. Since the original volatile content of Kīlauea's primary melt is unknown, we cannot further back-calculate the primary melt oxidation state. We note however, that the MI dataset explored here is likely to have captured most of the sulfur-degassing induced variation in melt oxidation state because this process typically occurs at shallow levels. The lower limit we provide is therefore likely to be fairly close to the oxidation state of the melt prior to degassing and points to a mantle source near the nickel nickel-oxide (NNO) buffer for Kīlauea's primary melt.

A parental mantle oxygen fugacity near NNO is at the oxidised end of values previously proposed for the Hawaiian mantle source. The suggestion that the initial oxygen fugacity of parental Hawaiian magmas is close to the MW buffer (Rhodes and Vollinger, 2005) is clearly irreconcilable with our data and an artefact of using the oxidation state of degassed basaltic glasses. Direct measurements of oxidation state of the lava lake (Fudali, 1965; Peck and Wright, 1966; Sato and Wright, 1966) and of erupted gases (Gerlach, 1980, 1993) point to conditions near QFM, closer to the primary magma oxygen fugacity as they record a mixed signal of more and less degassed magma. Oxygen fugacity conditions preserved by magnetite–ilmenite core equilibrium (Helz and Thornber, 1987) seem to faithfully preserve magmatic conditions near NNO, prior to degassing.

As a cautionary point, it is worth noting that the MI record used here is sampling melt that has experienced a significant amount of differentiation (around 40–45%; based on Clague et al., 1991). Starting with a melt at ΔNNO with 7 wt.% MgO and correcting for olivine fractionation up to a primary melt with 17 wt.% MgO using Petrolog3 (Danyushevsky and Plechov, 2011) and the mineral model of Herzberg and O'Hara (2002), for instance, would result in a primary melt at ∼ ΔQFM −0.2 (considering a closed system for oxygen). It is hence possible that Kīlauea's primary melt first experienced a net oxidation during differentiation followed by a net reduction during sulfur degassing. Since the melt inclusion record investigated here does not extend to such primary composition, the actual relationship, if any, between melt oxidation state and differentiation remains unresolved.

5. Conclusions

We performed X-ray absorption near-edge structure spectroscopy measurements at the iron K-edges on a series of olivine-hosted melt inclusions and matrix glasses from three historical eruptions at Kīlauea volcano. The main conclusions we draw from this study are:

1. Melt inclusions and matrix glasses at Kīlauea record a progressive reduction of the melt with degassing of volatile species.
2. The degassing of sulfur is likely the driving process behind this change, while H_2O and CO_2 degassing appear redox-neutral under the investigated conditions.
3. The oxidation state of Kīlauea's melt inclusions is consistent with measured volcanic gas compositions and points towards conditions of the parental mantle source close to the NNO buffer.

Our conclusions, whilst based on a case study at Kīlauea, should be widely applicable to basaltic systems in general. We therefore expect primary melts feeding OIBs to be more oxidised than recorded in their degassed, erupted products. MORBs, having lost sulfur, would also record a more reduced oxidation state than that of the undegassed melt. Arc basalts on the other hand have the potential to become progressively oxidised during degassing depending on their original oxidation state (i.e., they may have high initial S^{6+}/S_{tot} ratio). Using the oxidation state of erupted basalts as a direct reflection of their source mantle conditions can only be valid in the proven absence of sulfur degassing.

The discrepancy between the oxidation state of the gases and erupted basalts at Kīlauea shows that using the oxidation state of erupted lavas to infer the composition of their co-emitted gases can also be problematic.

Acknowledgements

We thank the Diamond Light Source for access to beamline I18 (proposal number SP11497-1) that contributed to the results presented here and the invaluable support during our analytical sessions from Konstantin Ignatyev. The Smithsonian Institution National Museum of Natural History is thanked for their loan of NMNH 117393. We thank Don Swanson (HVO-USGS) for his help acquiring the samples. YM acknowledges support from the Scripps Institution of Oceanography Postdoctoral Fellowship program. We are grateful to Nicole Métrich and an anonymous reviewer for providing valuable comments improving the quality of the manuscript. ME and CO are supported by the Natural Environment Research Council via the Centre for Observation and Modelling of Earthquakes, Volcanoes and Tectonics (COMET). NP is also funded by the Natural Environment Research Council (grant NE/N009312/1). NERC-funded studentship funded sample collection. ME acknowledges NERC ion probe grant IMF376/0509.

Appendix A. Supplementary material

Supplementary material related to this article can be found online at http://dx.doi.org/10.1016/j.epsl.2016.06.031.

References

Anderson, A.T., Wright, R., 1972. Phenocrysts and glass inclusions and their bearing on oxidation and mixing of basaltic magmas, Kilauea, Volcano. In: Hawaii 57, pp. 188–216.

Berry, et al., 2015. A reassessment of the oxidation state of iron in MORB glasses. In: Goldschmidt 2015. Praha. Abstract.

Bezos, A., Humler, E., 2005. The $Fe^{3+}/\sum Fe$ ratios of MORB glasses and their implications for mantle melting. Geochim. Cosmochim. Acta 69, 711–725.

Bottinga, Y., Javoy, M., 1990. MORB degassing: bubble growth and ascent. Chem. Geol. 81, 255–270.

Burgisser, A., Scaillet, B., 2007. Redox evolution of a degassing magma rising to the surface. Nature 445, 194–197.

Candela, P.A., 1986. The evolution of aqueous vapor from silicate melts: effect on oxygen fugacity. Geochim. Cosmochim. Acta 50, 1205–1211.

Carbone, D., Poland, M.P., 2012. Gravity fluctuations induced by magma convection at Kīlauea Volcano, Hawai'i. Geology 40, 803–806.

Carmichael, I.S., 1991. The redox states of basic and silicic magmas: a reflection of their source regions? Contrib. Mineral. Petrol. 106, 129–141.

Carmichael, I.S.E., Ghiorso, M.S., 1986. Oxidation–reduction relations in basic magma: a case for homogeneous equilibria. Earth Planet. Sci. Lett. 78, 200–210.

Carmichael, I.S.E., Ghiorso, M.S., 1990. The effect of oxygen fugacity on the redox state of natural liquids and their crystallizing phases. Rev. Mineral. Geochem. 24, 191–212.

Clague, D.A., Weber, W.S., Dixon, J.E., 1991. Picritic glasses from Hawaii. Nature 353, 553–556.

Cottrell, E., Kelley, K.A., 2011. The oxidation state of Fe in MORB glasses and the oxygen fugacity of the upper mantle. Earth Planet. Sci. Lett. 305, 270–282.

Cottrell, E., Kelley, K.A., 2013. Redox heterogeneity in mid-ocean ridge basalts as a function of mantle source. Science 340 (6138), 1314–1317. http://dx.doi.org/10.1126/science.1233299.

Cottrell, E., Kelley, K.A., Lanzirotti, A., Fischer, R.A., 2009. High-precision determination of iron oxidation state in silicate glasses using XANES. Chem. Geol. 268, 167–179.

Danyushevsky, L.V., Plechov, P., 2011. Petrolog3: integrated software for modeling crystallization processes. Geochem. Geophys. Geosyst. 12.

Dixon, J.E., Stolper, E., Delaney, J.R., 1988. Infrared spectroscopic measurements of CO_2 and H_2O in Juan de Fuca Ridge basaltic glasses. Earth Planet. Sci. Lett. 90, 87–104.

Edmonds, M., Gerlach, T.M., 2007. Vapor segregation and loss in basaltic melts. Geology 35, 751–754.

Edmonds, M., Sides, I.R., Swanson, D.A., Werner, C., Martin, R.S., Mather, T.A., Herd, R.A., Jones, R.L., Mead, M.I., Sawyer, G., Roberts, T.J., Sutton, A.J., Elias, T., 2013. Magma storage, transport and degassing during the 2008–10 summit eruption at Kīlauea Volcano, Hawai'i. Geochim. Cosmochim. Acta 123, 284–301.

Francis, P., Oppenheimer, C., Stevenson, D., 1993. Endogenous growth of persistently active volcanoes. Nature 366, 554–557.

Fudali, R.F., 1965. Oxygen fugacities of basaltic and andesitic magmas. Geochim. Cosmochim. Acta 29, 1063–1075.

Gaillard, F., Scaillet, B., 2009. The sulfur content of volcanic gases on Mars. Earth Planet. Sci. Lett. 279, 34–43.

Gaillard, F., Scaillet, B., Arndt, N.T., 2011. Atmospheric oxygenation caused by a change in volcanic degassing pressure. Nature 478, 229–232.

Gaillard, F., Scaillet, B., Pichavant, M., Iacono-Marziano, G., 2015. The redox geodynamics linking basalts and their mantle sources through space and time. Chem. Geol. 418, 217–233.

Gaillard, F., Schmidt, B., Mackwell, S., McCammon, C., 2003. Rate of hydrogen–iron redox exchange in silicate melts and glasses. Geochim. Cosmochim. Acta 67, 2427–2441.

Gerlach, T.M., 1980. Evaluation of volcanic gas analyses from Kilauea volcano. J. Volcanol. Geotherm. Res. 7, 295–317.

Gerlach, T.M., 1986. Exsolution of H_2O, CO_2, and S during eruptive episodes at Kilauea Volcano, Hawaii. J. Geophys. Res., Solid Earth 91, 12177–12185.

Gerlach, T.M., 1993. Oxygen buffering of Kilauea volcanic gases and the oxygen fugacity of Kilauea basalt. Geochim. Cosmochim. Acta 57 (4), 795–814.

Gerlach, T.M., 2004. Comment on paper: 'Morphology and compositions of spinel in Pu'u 'Ō'ō lava (1996–1998), Kilauea volcano, Hawaii'–enigmatic discrepancies between lava and gas-based fO_2 determinations of Pu'u 'Ō'ō lava. J. Volcanol. Geotherm. Res. 134, 241–244.

Hauri, E., 2002. SIMS analysis of volatiles in silicate glasses, 2: isotopes and abundances in Hawaiian melt inclusions. Chem. Geol. 183, 115–141.

Helz, R.T., 2009. Reduction of basaltic melt during near-surface evolution of SO_2: a possible example from Kilauea. In: GSA Annual Meeting 2009. Portland. Abstract.

Helz, R.T., Thornber, C.R., 1987. Geothermometry of Kilauea Iki lava lake, Hawaii. Springer. Bull. Volcanol. 49, 651–668.

Herzberg, C., O'Hara, M.J., 2002. Plume-associated ultramafic magmas of phanerozoic age. J. Petrol. 43, 1857–1883.

Holloway, J.R., 2004. Redox reactions in seafloor basalts: possible insights into silicic hydrothermal systems. Chem. Geol. 210, 225–230.

Humphreys, M.C.S., Brooker, R.A., Fraser, D.G., Burgisser, A., Mangan, M.T., McCammon, C., 2015. Coupled interactions between volatile activity and Fe oxidation state during arc crustal processes. J. Petrol., egv017.

Iacono-Marziano, G., Morizet, Y., Le Trong, E., Gaillard, F., 2012. New experimental data and semi-empirical parameterization of H_2O–CO_2 solubility in mafic melts. Geochim. Cosmochim. Acta 97, 1–23.

Kelley, K.A., Cottrell, E., 2012. The influence of magmatic differentiation on the oxidation state of Fe in a basaltic arc magma. Earth Planet. Sci. Lett. 329–330, 109–121.

Kress, V.C., Carmichael, I.S.E., 1991. The compressibility of silicate liquids containing Fe_2O_3 and the effect of composition, temperature, oxygen fugacity and pressure on their redox states. Contrib. Mineral. Petrol. 108, 82–92.

Lee, C., Leeman, W.P., Canil, D., Li, Z., 2005. Similar V/Sc systematics in MORB and arc basalts: implications for the oxygen fugacities of their mantle source regions. J. Petrol. 46, 2313–2336.

Mather, T.A., Witt, M.L.I., Pyle, D.M., Quayle, B.M., Aiuppa, A., Bagnato, E., Martin, R.S., Sims, K.W.W., Edmonds, M., Sutton, A.J., Ilyinskaya, E., 2012. Halogens and trace metal emissions from the ongoing 2008 summit eruption of Kīlauea volcano, Hawai'i. Geochim. Cosmochim. Acta 83, 292–323.

Mathez, E.A., 1984. Influence of degassing on oxidation states of basaltic magmas. Nature 310, 371–375.

Métrich, N., Berry, A.J., O'Neill, H.S.C., Susini, J., 2009. The oxidation state of sulfur in synthetic and natural glasses determined by X-ray absorption spectroscopy. Geochim. Cosmochim. Acta 73, 2382–2399.

Moore, J.G., 1979. Vesicularity and CO_2 in mid-ocean ridge basalt. Nature 282, 250–253.

Moussallam, Y., Oppenheimer, C., Scaillet, B., Buisman, I., Kimball, C., Dunbar, N., Burgisser, A., Ian Schipper, C., Andújar, J., Kyle, P., 2015. Megacrystals track magma convection between reservoir and surface. Earth Planet. Sci. Lett. 413, 1–12.

Moussallam, Y., Oppenheimer, C., Scaillet, B., Gaillard, F., Kyle, P., Peters, N., Hartley, M., Berlo, K., Donovan, A., 2014. Tracking the changing oxidation state of Erebus magmas, from mantle to surface, driven by magma ascent and degassing. Earth Planet. Sci. Lett. 393, 200–209.

O'Neill, H.S.C., Mavrogenes, J.A., 2002. The sulfide capacity and the sulfur content at sulfide saturation of silicate melts at 1400 °C and 1 bar. J. Petrol. 43, 1049–1087.

Patrick, M.R., Orr, T., Wilson, D., Dow, D., Freeman, R., 2011. Cyclic spattering, seismic tremor, and surface fluctuation within a perched lava channel, Kīlauea Volcano. Bull. Volcanol. 73, 639–653.

Peck, D., Wright, T.L., 1966. Experimental studies of molten basalt in situ; a summary of physical and chemical measurements on recent lava lakes of Kilauea Volcano, Hawaii. Geol. Soc. Am. Annu. Meet. 101.

Pichavant, M., Carlo, I.D., Rotolo, S.G., Scaillet, B., Burgisser, A., Gall, N.L., Martel, C., 2013. Generation of CO_2-rich melts during basalt magma ascent and degassing. Contrib. Mineral. Petrol. 166, 545–561.

Rhodes, J.M., Vollinger, M.J., 2005. Ferric/ferrous ratios in 1984 Mauna Loa lavas: a contribution to understanding the oxidation state of Hawaiian magmas. Contrib. Mineral. Petrol. 149, 666–674.

Roeder, P.L., Thornber, C., Grant, A., 2004. Reply to comment on paper: "Morphology and composition of spinel in Pu'u 'Ō'ō lava (1996–1998), Kilauea volcano, Hawaii"—enigmatic discrepancies between lava and gas-based fO_2 determinations of Pu'u 'Ō'ō lava. J. Volcanol. Geotherm. Res. 134, 245–248.

Roeder, P.L., Thornber, C., Poustovetov, A., Grant, A., 2003. Morphology and composition of spinel in Pu'u 'Ō'ō lava (1996–1998), Kilauea Volcano, Hawaii. J. Volcanol. Geotherm. Res. 123, 245–265.

Sato, M., 1978. Oxygen fugacity of basaltic magmas and the role of gas-forming elements. Geophys. Res. Lett. 5, 447–449.

Sato, M., Wright, T.L., 1966. Oxygen fugacities directly measured in magmatic gases. Science 153, 1103–1105.

Shorttle, O., Moussallam, Y., Hartley, M.E., Maclennan, J., Edmonds, M., Murton, B.J., 2015. Fe-XANES analyses of Reykjanes Ridge basalts: implications for oceanic crust's role in the solid Earth oxygen cycle. Earth Planet. Sci. Lett. 427, 272–285.

Sides, I.R., Edmonds, M., Maclennan, J., Swanson, D.A., Houghton, B.F., 2014. Eruption style at Kīlauea Volcano in Hawai'i linked to primary melt composition. Nat. Geosci. 7, 464–469.

Tazieff, H., 1994. Permanent lava lakes: observed facts and induced mechanisms. J. Volcanol. Geotherm. Res. 63, 3–11.

Wallace, P.J., Anderson, A.T., 1998. Effects of eruption and lava drainback on the H_2O contents of basaltic magmas at Kilauea Volcano. Bull. Volcanol. 59, 327–344.

Waters, L.E., Lange, R.A., 2016. No effect of H_2O degassing on the oxidation state of magmatic liquids. Earth Planet. Sci. Lett. 447, 48–59.

Wilke, M., Jugo, P.J., Klimm, K., Susini, J., Botcharnikov, R., Kohn, S.C., Janousch, M., 2008. The origin of S^{4+} detected in silicate glasses by XANES. Am. Mineral. 93, 235–240.

Wright, T.L., Weiblen, P., 1968. Mineral composition and paragenesis in tholeiitic basalt from Makaopuhi lava lake, Hawaii. Spec. Pap., Geol. Soc. Am., 242–243.